Functional Materials

DOI: 10.1002/ange.201305590

Strongly Phosphorescent Palladium(II) Complexes of Tetradentate Ligands with Mixed Oxygen, Carbon, and Nitrogen Donor Atoms: Photophysics, Photochemistry, and Applications**

*Pui Keong Chow, Chensheng Ma, Wai-Pong To, Glenna So Ming Tong, Shiu-Lun Lai, Steven C. F. Kui, Wai-Ming Kwok, and Chi-Ming Che**

Transition-metal complexes that show strong phosphorescence in solution at room temperature usually contain a Ru^{II}, Os^{II}, Ir^{III}, or Pt^{II} ion, but luminescent Au^{III} complexes[1] have also been studied increasingly. In contrast to the extensive literature on luminescent Pt^{II} complexes,[2] examples of luminescent Pd^{II} complexes that contain non-porphyrin ligands and show decent emission quantum yields (Φ_{em}) are sparse.[3] The crux of this long-standing situation lies in the significantly lower ligand-field splitting of the Pd^{II} ion.[4] Accordingly, the metal-centered d–d states of Pd^{II} complexes are always thermally accessible, which enables facile population of the antibonding $4d_{x^2-y^2}$ orbital and hence leads to effective nonradiative decay through severe excited-state structural distortion.

A strategy for suppression of the d–d deactivation is to use strong-field ligands so as to raise the d–d states to a higher energy. Although many bidentate and tridentate chelating ligands, such as C-deprotonated C^N and C^N^N (HC^N = 2-phenylpyridine; HC^N^N = 6-phenyl-2,2′-bipyridine) ligands, give luminescent Pt^{II} complexes, they are not effective for the design of luminescent Pd^{II} complexes. Most of the reported luminescent Pd^{II} complexes containing non-porphyrin ligands are only weakly emissive ($\Phi_{em} <$ ca. 10^{-2}) at low temperature (77 K)[4] and non-emissive ($\Phi_{em} <$ ca. 10^{-4}) in solution at room temperature.[3] Notable examples of phosphorescent Pd^{II} complexes include Pd^{II}–porphyrin complexes ($\lambda_{max} = 668$–797 nm; Φ_{em} up to 0.45) and Pd^{II}–Schiff base complexes ($\lambda_{max} = 762$–792 nm; Φ_{em} up to 0.023),[5] the emitting excited states of both of which are lower-lying than the d–d states. Thus, we asked the question: is it possible to prepare strongly luminescent Pd^{II} complexes with d–d excited states that are thermally inaccessible from the emissive ^{3}IL (intraligand) and/or ^{3}MLCT (metal-to-ligand charge transfer) excited states and which are efficient blue- or green-light emitters?

Herein we report a new class of Pd^{II} complexes containing tetradentate O^N^C^N ligands (Scheme 1). These complexes emit green light (at ca. 530 nm) and exhibit high Φ_{em} values of up to 0.22 and long emission lifetimes (τ_o) of up to about 120 μs in solution at room temperature. The series of ligands were designed by the incorporation of a σ-donating phenolate (phol) group tethered to one pyridyl ring (PyA) of the N^C^N moiety either through a single covalent bond (complexes **1**–**3**, type I) or through a methylene bridge (complexes **4**–**8**, type II). These O^N^C^N ligands are strong σ donors, strongly destabilize the antibonding Pd^{II} $4d_{x^2-y^2}$ orbital, and can impart robustness and thermal stability to the corresponding Pd^{II} complexes for practical applications in materials. The structural rigidity of the O^N^C^N ligand scaffold facilitates emission at relatively high energy and prevents nonradiative decay resulting from ligand distortion.

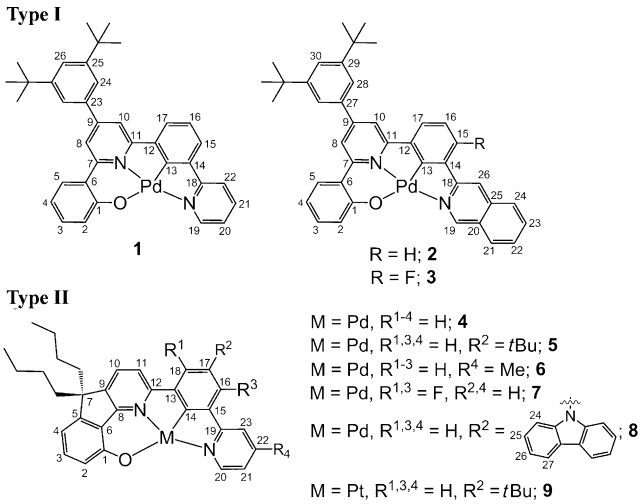

Scheme 1. Structures of the Pd^{II} and Pt^{II} complexes **1**–**9**.

[*] P. K. Chow, Dr. C. Ma, Dr. W.-P. To, Dr. G. S. M. Tong, Dr. S.-L. Lai, Dr. S. C. F. Kui, Prof. Dr. C.-M. Che
State Key Laboratory of Synthetic Chemistry, Institute of Molecular Functional Materials, HKU-CAS Joint Laboratory on New Materials and
Department of Chemistry, The University of Hong Kong
Pokfulam Road, Hong Kong (China)
E-mail: cmche@hku.hk
Prof. Dr. C.-M. Che
HKU Shenzhen Institute of Research and Innovation
Shenzhen 518053 (China)
Dr. W.-M. Kwok
Department of Applied Biology and Chemical Technology
The Hong Kong Polytechnic University
Hung Hom, Kowloon, Hong Kong (China)

[**] This research was supported by the Area of Excellence Scheme AoE/P-03/08, the National Key Basic Research Program of China (No. 2013CB834802), and the CAS-Croucher Foundation Funding Scheme for Joint Laboratories

Supporting information for this article is available on the WWW under http://dx.doi.org/10.1002/anie.201305590.

Pt^{II} complexes of O^N^C^N ligands have been reported to display high emission quantum yields.[6]

Details of the synthesis and characterization of the Pd^{II} complexes **1**–**8** and a type II Pt^{II} analogue **9** are given in the Supporting Information. The X-ray crystal structures of **1**, **4**, and **7** were determined (see the Supporting Information for details). In both **1** and **4**, the Pd atom adopts a distorted square planar geometry with N-Pd-N angles of 160.1(5)–162.0(9)°. The Pd–C (C donor in the O^N^C^N ligand) and Pd–N distances are 1.909(2)–1.984(4) and 1.982(1)–2.061(3) Å, respectively, and are thus similar to those reported for Pd^{II} and Pt^{II} complexes with a N^C^N ligand.[7] The Pd–O distances are 2.048(3)–2.116(5) Å, slightly longer than those in the complex $[Pd(N^N)(OPh)_2]$ (N^N = bipyridine, 1.983–1.996 Å).[8]

The steady-state absorption and emission spectra of **1** and **5** in dichloromethane are depicted in Figure 1 with key spectral parameters listed in Table 1. The spectral data obtained in other solvents are listed in Table S3 in the Supporting Informaton. All of the complexes exhibit intense absorption bands at 250–320 nm ($\varepsilon = 4$–$7 \times 10^4\ dm^3\,mol^{-1}\,cm^{-1}$), moderately intense absorption bands with $\lambda_{max} \approx 350$ nm ($\varepsilon = 1$–$2 \times 10^4\ dm^3\,mol^{-1}\,cm^{-1}$), and relatively weak absorptions at 370–450 nm ($\varepsilon = 3$–$5 \times 10^3\ dm^3\,mol^{-1}\,cm^{-1}$). The absorption bands at 250–320 nm and approximately 350 nm resemble those of the corresponding free ligands. The absorptions at approximately 370–450 nm show a moderate negative solvatochromic shift (e.g. for **1**, from ca. 411 nm in acetonitrile to ca. 431 nm in hexane; see Figure S11 in the Supporting Information) and are attributed, according to density functional theory (DFT) and time-dependent DFT (TDDFT) calculations, to an admixture of LLCT (ligand-to-ligand charge transfer; $\pi_{phol} \rightarrow \pi^*_{N^C^N}$) and MLCT ($d\pi \rightarrow \pi^*_{O^N^C^N}$) transitions. The inclusion of $d\pi \rightarrow \pi^*$ MLCT is in line with the red shift of the lowest-energy absorption band from **5** (410 nm) to its Pt^{II} congener **9** (430 nm) in dichloromethane, an observation expected on the basis of the lower oxidation potential of Pt^{II} relative to that of the Pd^{II} ion.[4a]

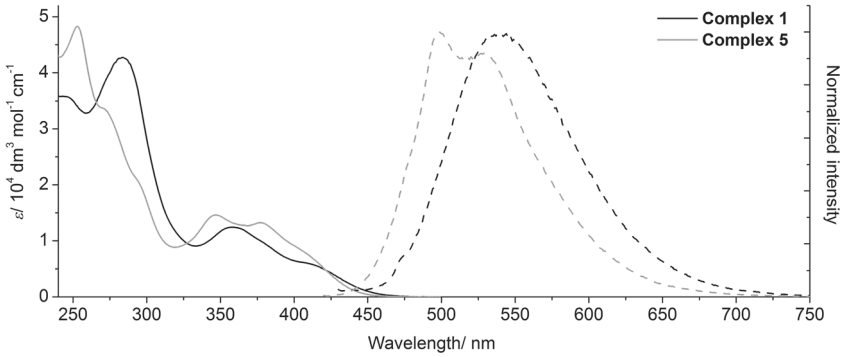

Figure 1. Absorption (solid lines) and emission spectra (dashed lines) of **1** (black lines) and **5** (gray lines) in dichloromethane at 298 K.

Table 1: Emission data of complexes **1**–**9** in dichloromethane.

Complex	λ_{max} [nm]	τ_o [μs][a]	Φ_{em}[b]	k_r [$10^3\ s^{-1}$][c]	k_{nr} [$10^3\ s^{-1}$][d]
1	540	0.4	0.0019	48	2500
2	543	0.2	0.002	10	5000
3	535	< 0.2	0.0016	–[e]	–[e]
4	527	105	0.15	1.4	8.1
5	498	121	0.20	1.7	6.6
6	527	122	0.17	1.4	6.8
7	517	62	0.22	3.5	13
8	536	83	0.14	1.7	10
9	537	10	0.79	77	20

[a] Emission lifetime at λ_{max}. [b] Emission quantum yield measured at 1×10^{-5} mol dm^{-3} at room temperature with $[Ru(bpy)_3](PF_6)_2$ (bpy = 2,2′-bipyridine) in degassed acetonitrile as a standard ($\Phi_{em} = 0.062$). [c] Radiative-decay rate constant estimated from the equation $k_r = \Phi/\tau$. [d] Nonradiative-decay rate constant estimated from the equation $k_{nr} = (1-\Phi)/\tau$. [e] The value was not estimated, as the short emission lifetime of **3** (< 0.2 μs) is beyond the detection limit of our instrument.

Type I complexes are weakly emissive ($\Phi_{em} \approx 0.002$) with rather short emission lifetimes ($\tau \approx 0.2$–0.4 μs) and structureless emission bands ($\lambda_{max} \approx 535$–$543$ nm) that display a sizeable red shift in energy as the solvent polarity increases (e.g. from 506 nm in hexane to 549 nm in acetonitrile in the case of **1**; see Figure S12). Type II complexes are strongly emissive ($\Phi_{em} \approx 0.14$–0.22 for **4**–**8**; $\Phi_{em} \approx 0.79$ for the Pt^{II} congener **9**) with notably longer emission lifetimes ($\tau \approx 83$–122 μs for **4**–**8**; $\tau \approx 10$ μs for **9**). Complexes **4**–**6** and **9** show structured emission profiles with vibrational progressions of about 1200–1600 cm^{-1} attributed to the ligand C=C and/or C=N stretching vibrations. The emissions of all type II complexes remain little changed upon variation of the solvent polarity (e.g. from 516 nm in hexane to 526 nm in acetonitrile in the case of **4**; see Figure S12). As revealed by the DFT/TDDFT calculations, the emissions of the type I and type II Pd^{II} complexes arise from the lowest-energy triplet excited states (T_1) of $^3LLCT(\pi_{phol} \rightarrow \pi^*_{N^C^N})$ and N^C^N-localized $^3IL(\pi \rightarrow \pi^*)$ in parentage, respectively, both with less than 10% $^3MLCT(d\pi \rightarrow \pi^*)$ character. The self-quenching rate constants of these emissions are on the order of $10^7\ dm^3\,mol^{-1}\,s^{-1}$ for **4**, **5**, and **9**, and thus notably lower than the values of approximately $10^9\ dm^3\,mol^{-1}\,s^{-1}$ reported for the related complex $[Pt^{II}(N^C^N)Cl]$. Presumably the long alkyl chains of O^N^C^N ligands disfavor intermolecular close contact of the Pd^{II} and Pt^{II} complexes.

DFT and TDDFT calculations performed on the type I complex **1** and type II complexes **5** and **9** at their respective optimized ground-state (S_0) and T_1 geometries showed that as a result of the distinct electronic character of the T_1 state in the two types of complexes ($^3LLCT(\pi \rightarrow \pi^*)$ for type I versus $^3IL(\pi \rightarrow \pi^*)$ for type II; Figure 2), the T_1 state of **1** and that of **5** or **9** (^3IL) feature different geometry with respect to that of the corresponding S_0 state. The structures of **5** and **9** remain coplanar at both optimized S_0 and T_1 states. However, in the case of **1**, there is significant structural distortion upon the transition from S_0 to T_1; the dihedral angle (δC1-C6-C7-N) between the phenolate ring and the pyridine ring of the O^N^C^N ligand changes from approximately 37° at the

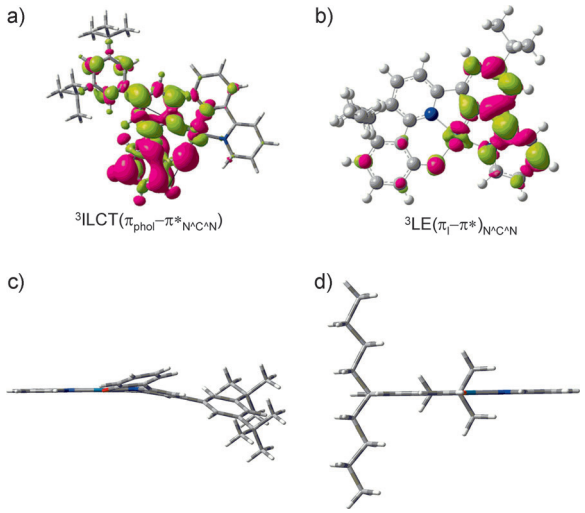

Figure 2. a,b) Calculated electron difference density maps of the lowest-energy triplet excited state (black: decrease in electron density; gray: increase in electron density) of **1** (a) and **5** (b). c,d) Structures of the T_1 state of **1** (c) and **5** (d).

optimized S_0 state to approximately 26° at the optimized T_1 state. For both type I and type II complexes, there is no low-lying d–d* excited state in either the singlet or the triplet manifold in the excitation-energy range used in the spectroscopic study.

Femtosecond (fs) broadband time-resolved fluorescence (TRF) and transient absorption (TA) experiments on **1**, **5**, and **9** revealed similar patterns of excited-state cascades but with different rates of singlet-to-triplet intersystem crossing (ISC; k_{isc}) and different rates of decay of T_1 to S_0 through radiative (k_r) and nonradiative processes (k_{nr}). Typical data acquired for **5** are displayed in Figure 3 (for the corresponding results for **1** and **9**, see Figures S13 and S14).

Upon excitation at 380 nm, **5** exhibited instantaneous TRF (0.1 ps) at $\lambda_{max} \approx 460$ nm from an electronically excited singlet state, which decayed with an accompanying dynamic Stokes shift (DSS; to $\lambda_{max} \approx 510$ nm by 3 ps) and disappeared by about 50 ps after excitation (Figure 3a). Analysis of the kinetic decay of the TRF intensity (see the Supporting Information for details) revealed biexponential dynamics with time constants of approximately 0.7 and 10.3 ps (Figure 3c). The time constant of approximately 0.7 ps is close to the time constant (ca. 0.8 ps) that describes the DSS (inset in Figure 3c) and can be understood to arise mainly from structural and vibrational relaxation of the initial singlet excited state upon photopopulation to evolve to its energy minimum.

The TA recorded for **5** at 0.1 ps after fs laser excitation shows a broad spectrum with the evolution of the band at $\lambda_{max} \approx 450$ nm according to a time constant of approximately 10.7 ps (Figure 3d) into a different profile featuring $\lambda_{max} \approx 435/510$ nm and an isosbestic point at approximately 480 nm (Figure 3b). This spectral evolution implies a precursor–successor relationship between the TA at approximately 450 nm and that at about 435/510 nm. The TA at 435/510 nm is long-lived and persists with no change in intensity over a longer timescale from 40 ps to 6 ns (inset in Figure 3d; see also Figure S15). The dynamics of TA with 10.7 ps time constant matches well with the TRF time constant of approximately 10.3 ps. The long-lived species, which has a much lower radiative-decay rate than that of the singlet excitation (as suggested by the lack of a corresponding long-lived component in the fs-TRF) was ascribed to the T_1 state (^{3}IL($\pi \rightarrow \pi^*$)), an assignment which was further verified by a nanosecond time-resolved emission measurement (see Figure S16). We therefore assign the approximately 10 ps process to singlet-to-triplet ISC with an ISC time constant (τ_{isc}) of about 10 ps and an ISC rate constant (k_{isc}) of ca. 10^{11} s^{-1}. Parallel TR studies revealed that **1** and **9** feature ISC time constants of about 33 and 0.12 ps, respectively. In

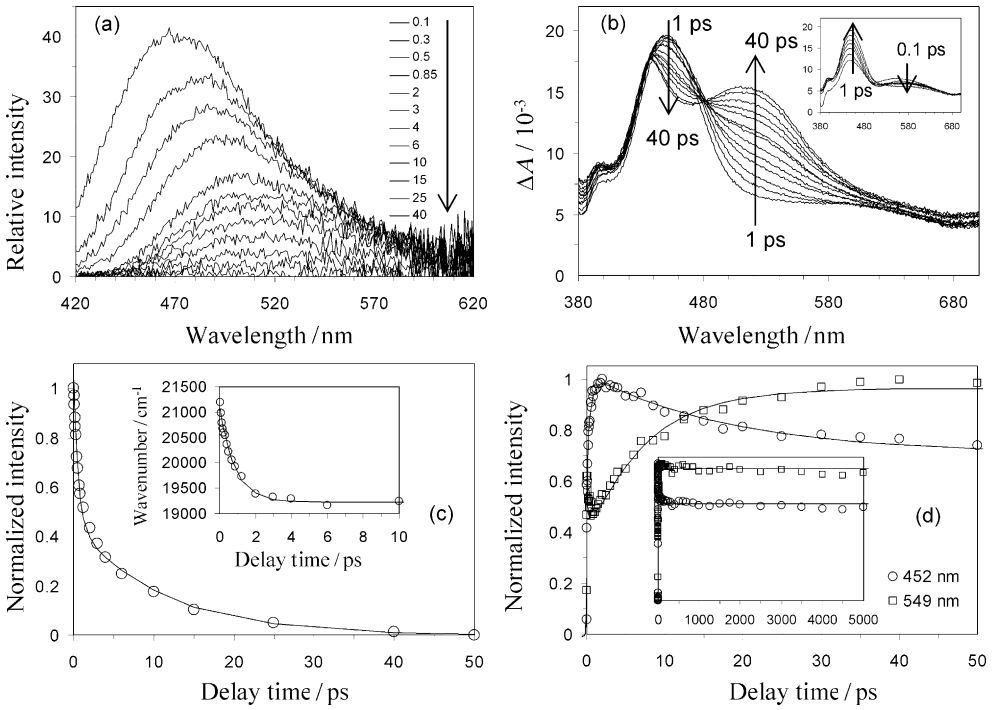

Figure 3. a,b) Temporal evolution of fs-TRF (a) and fs-TA (b) at the denoted time intervals (in picoseconds) after the excitation of **5** at 380 nm in dichloromethane. The arrows show the direction of spectral evolution. c,d) Normalized experimental (○, □) and fitted (lines) time profiles for TRF decay (c) and TA (d) at the denoted wavelengths in the TRF and TA spectra. The inset in (c) shows the time dependence of the TRF λ_{max} value in the spectra in (a); the inset in (d) displays TA time profiles at time intervals from 0.1 to 6000 ps after excitation.

comparison to the value for **5** ($\tau_{isc} \approx 10$ ps), the about 100-fold faster ISC in the case of **9** is not surprising if the heavy-atom effect that promotes spin–orbit coupling (SOC constant $\xi =$ 1412/4000 cm^{-1} for Pd^{II}/Pt^{II}) is taken into account; the slower ISC in **1** shows that a subtle change in ligand structure can notably alter the ISC rate. The ISC rates of the three complexes are all very high and greatly exceed the radiative rates of the singlet emission (ca. $10^8\ s^{-1}$). These rates suggest a close-to-unitary ISC quantum efficiency ($\Phi_{isc} \approx 1$) and account for the apparent lack of fluorescence emission in the corresponding steady-state spectra (Figure 1). They also indicate that the phosphorescence quantum yields of the Pd^{II} complexes are governed solely by the dynamic competition of the radiative (k_r) versus the nonradiative decay (k_{nr}) of the emitting triplet state. The values of k_r and k_{nr} derived from the measured Φ_{em} and τ_0 values are included in Table 1.

The root cause for the high Φ_{em} and long τ_0 values of **5** and all the other type II Pd^{II} complexes (**4**, **6**–**8**) is their modest k_r value (ca. $1.4–3.5 \times 10^3\ s^{-1}$) coupled with a similarly low k_{nr} value (ca. $6.4–10 \times 10^3\ s^{-1}$); the much lower/shorter Φ_{em}/τ_0 values exhibited by type I complexes (**1**–**3**) are primarily a result of their about 500-fold higher k_{nr} value (ca. $2.5 \times 10^6\ s^{-1}$) combined with a slightly higher k_r value. The modest radiative rate k_r shown by type II Pd^{II} complexes is an intrinsic result of the small metal contribution (9% according to DFT) in the $^3IL(\pi\rightarrow\pi^*)$ T_1 excitation of these complexes; the favorable low rate k_{nr} in this system is in line with the similar coplanar structures of the T_1 to S_0 states. Thus, providing that type I and II Pd^{II} complexes are both free from d–d* deactivation (as suggested by DFT), the much faster rate k_{nr} of type I complexes is caused by ligand deformation in the nonplanar T_1 state and the ^3LLCT T_1 parentage, both of which are not present in the $^3IL(\pi\rightarrow\pi^*)$ T_1 excited states of the strictly coplanar type II complexes.

The high emission quantum yields and long lifetimes of the triplet excited states suggest a range of promising applications, four of which are highlighted below.

1) The type II Pd^{II} complexes are good luminescent oxygen sensors. For example, we observed a greater than 300-fold decrease in emission intensity (at $\lambda_{max} \approx 530$ nm) upon the exposure of a solution of **5** in dichloromethane to air; this decrease in emission intensity corresponds to a rate constant (k_q) of emission quenching by oxygen of about $2.5 \times 10^9\ s^{-1}$.

2) In deoxygenated solutions of the Pd^{II} complexes **4**–**8** with 9,10-diphenylanthracene (DPA) in dichloromethane, excitation with a 355 nm laser light (Nd:YAG laser) gave rise to both prompt and delayed fluorescence of DPA (5×10^{-5} mol dm^{-3}) together with minor phosphorescence of the Pd^{II} complex (2×10^{-5} mol dm^{-3}).[9] Upon excitation, the Pd^{II} complex in its long-lived triplet excited state reacts with DPA by energy transfer to produce triplet-excited DPA ($^3DPA^*$), which undergoes a bimolecular triplet–triplet annihilation (TTA) reaction to give a singlet-excited DPA molecule ($^1DPA^*$) and a ground-state DPA molecule. The relaxation of $^1DPA^*$ to its ground state gives rise to the observed delayed fluorescence (Figure 4) with delayed fluorescence quantum yields estimated to be 14–21% (see Table S4).

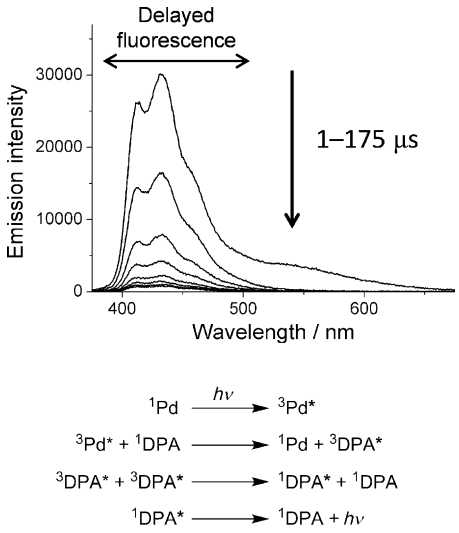

Figure 4. Top: Time-resolved emission spectra of a mixture of **7** (2×10^{-5} mol dm^{-3}) and DPA (5×10^{-5} mol dm^{-3}) in degassed dichloromethane as recorded from 1 to 175 µs after laser pulse excitation (355 nm). The arrow indicates the change in emission intensity. Bottom: Mechanism of TTA-based delayed fluorescence.

3) Another application of these complexes is in light-induced oxidative C–H functionalization reactions.[10] In this study, **4**–**8** were found to be capable of catalyzing the oxidation of secondary amines by oxygen under light irradiation (Scheme 2; see also Table S5). Complex **8** dis-

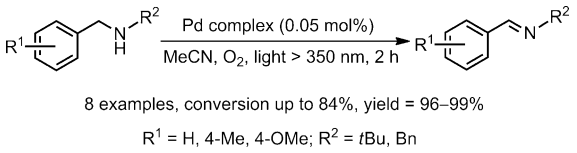

Scheme 2. Photochemical reactions catalyzed by the Pd^{II} complexes. Bn = benzyl.

played the highest activity and furnished the products with up to about 1650 turnovers in 2 h (see Table S5, entry 6). Singlet oxygen sensitized by the triplet-excited Pd^{II} complex is proposed to be the active oxidant.[11] This finding reveals that Pd^{II} complexes containing non-porphyrin ligands may also possess rich photochemical properties analogous to those displayed by their Pt^{II} counterparts.

4) The application of **5** (decomposition temperature: 418 °C) in organic light-emitting diodes (OLEDs) was also examined. Complex **5** was vacuum-deposited as a dopant into the emissive material layer of an OLED with the configuration ITO/NPB (40 nm)/*x* % **5**: mCP (30 nm)/BAlq (40 nm)/LiF (0.5 nm)/Al (80 nm; see the Supporting Information for details of OLED fabrication; ITO = indium tin oxide, NPB = *N*,*N*′-di(1-naphthyl)-*N*,*N*′-diphenyl-1,1′-biphenyl-4,4′-diamine, mCP = 1,3-bis(*N*-carbazolyl)benzene, BAlq = bis(2-methyl-8-quinolato)-(4-phenylphenolate)aluminum). Figure 5a shows the normalized electroluminescence (EL) spectra of the OLEDs at a luminance of 100 cd m^{-2} with various dopant concentrations of **5**. The EL

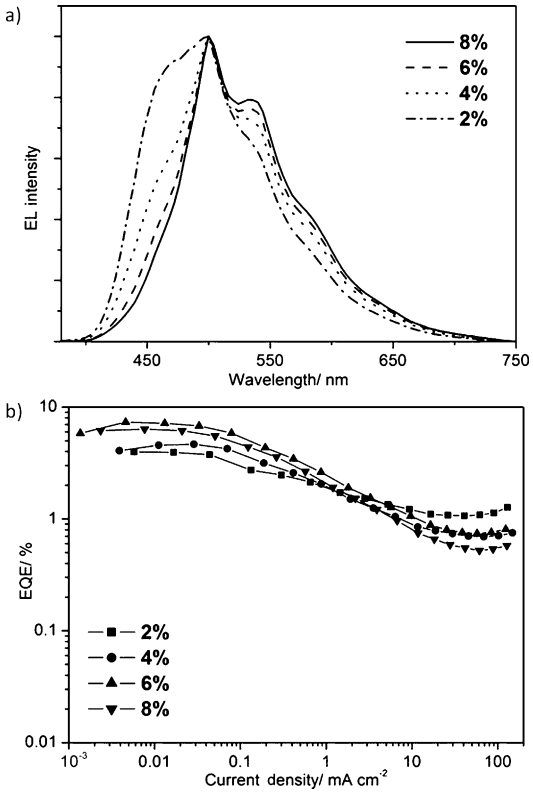

Figure 5. a) EL spectra of the devices with different concentrations of **5** doped into the mCP layer at a luminance of 100 cd m^{-2}. b) Plots of the external quantum efficiency (EQE) of the devices with **5** at different dopant concentrations versus current density.

spectrum of the device with a 6% dopant concentration showed emission maxima at 500, 535, and 589 nm, the CIE coordinates (0.27, 0.44), a maximum current density of 20.0 cd A^{-1}, and a maximum power efficiency of 13.6 Lm W^{-1} (see Figure S17). Plots of the external quantum efficiency (EQE) of devices with **5** at different dopant concentrations versus current density are depicted in Figure 5b. With this simple device structure, a maximum EQE of 7.4% was reached, which is comparable to the EQE of recently reported OLEDs based on Pt^{II} complexes.[12]

In conclusion, a series of Pd^{II} complexes supported by tetradentate O^N^C^N ligands exhibited unprecedentedly high emission quantum yields in the 510–550 nm spectral region in solution at room temperature. These complexes showed good performance in photocatalysis and displayed promise for effective applications in materials. The discovery of this class of luminescent Pd^{II} complexes, which show strong green phosphorescence, indicates the usefulness of tetradentate ligand systems with a rigid scaffold and strong donor atoms in the development of highly robust and strongly phosphorescent metal-based emitters.

Received: June 28, 2013
Published online: September 20, 2013

Keywords: organic light-emitting diodes · palladium · phosphorescence · photochemistry · tetradentate ligands

[1] a) C. Bronner, O. S. Wenger, *Dalton Trans.* **2011**, *40*, 12409 – 12420; b) V. K.-M. Au, K. M.-C. Wong, N. Zhu, V. W.-W. Yam, *Chem. Eur. J.* **2011**, *17*, 130 – 142; c) W.-P. To, G. S. M. Tong, W. Lu, C. Ma, J. Liu, A. L.-F. Chow, C.-M. Che, *Angew. Chem.* **2012**, *124*, 2708 – 2711; *Angew. Chem. Int. Ed.* **2012**, *51*, 2654 – 2657; d) D.-A. Roşca, D. A. Smith, M. Bochmann, *Chem. Commun.* **2012**, *48*, 7247 – 7249; e) V. K.-M. Au, N. Zhu, V. W.-W. Yam, *Inorg. Chem.* **2013**, *52*, 558 – 567; f) W.-P. To, K. T. Chan, G. S. M. Tong, C. Ma, W.-M. Kwok, X. Guan, K.-H. Low, C.-M. Che, *Angew. Chem.* **2013**, *125*, 6780 – 6784; *Angew. Chem. Int. Ed.* **2013**, *52*, 6648 – 6652.

[2] a) S.-W. Lai, C.-M. Che, *Top. Curr. Chem.* **2004**, *241*, 27 – 63; b) J. A. G. Williams, *Top. Curr. Chem.* **2007**, *281*, 205 – 268; c) M. L. Muro, A. A. Rachford, X. Wang, F. N. Castellano, *Top. Organomet. Chem.* **2010**, *29*, 159 – 191; d) S. C. F. Kui, P. K. Chow, G. Cheng, C.-C. Kwok, C. L. Kwong, K.-H. Low, C.-M. Che, *Chem. Commun.* **2013**, *49*, 1497 – 1499.

[3] a) M. Ghedini, I. Aiello, M. La Deda, A. Grisolia, *Chem. Commun.* **2003**, 2198 – 2199; b) V. A. Kozlov, D. V. Aleksanyan, Y. V. Nelyubina, K. A. Lyssenko, E. I. Gutsul, L. N. Puntus, A. A. Vasil'ev, P. V. Petrovskii, I. L. Odinets, *Organometallics* **2008**, *27*, 4062 – 4070; c) S. M. Borisov, G. Zenkl, I. Klimant, *ACS Appl. Mater. Interfaces* **2010**, *2*, 366 – 374; d) C. Bronner, S. A. Baudron, M. W. Hosseini, C. A. Strassert, A. Guenet, L. De Cola, *Dalton Trans.* **2010**, *39*, 180 – 184.

[4] a) S.-W. Lai, T.-C. Cheung, M. C. W. Chan, K.-K. Cheung, S.-M. Peng, C.-M. Che, *Inorg. Chem.* **2000**, *39*, 255 – 262; b) F. Neve, A. Crispini, C. Di Pietro, S. Campagna, *Organometallics* **2002**, *21*, 3511 – 3518; c) M. Ghedini, T. Pugliese, M. La Deda, N. Godbert, I. Aiello, M. Amati, S. Belviso, F. Lelj, G. Accorsi, F. Barigelletti, *Dalton Trans.* **2008**, 4303 – 4318; d) J. Kuwabara, Y. Ogawa, A. Taketoshi, T. Kanbara, *J. Organomet. Chem.* **2011**, *696*, 1289 – 1293.

[5] a) A. Y. Lebedev, M. A. Filatov, A. V. Cheprakov, S. A. Vinogradov, *J. Phys. Chem. A* **2008**, *112*, 7723 – 7733; b) S. M. Borisov, R. Saf, R. Fischer, I. Klimant, *Inorg. Chem.* **2013**, *52*, 1206 – 1216.

[6] S. C. F. Kui, P. K. Chow, G. S. M. Tong, S.-L. Lai, G. Cheng, C.-C. Kwok, K.-H. Low, M. Y. Ko, C.-M. Che, *Chem. Eur. J.* **2013**, *19*, 69 – 73.

[7] a) B. Soro, S. Stoccoro, G. Minghetti, A. Zucca, M. A. Cinellu, S. Gladiali, M. Manassero, M. Sansoni, *Organometallics* **2005**, *24*, 53 – 61; b) D. J. Cárdenas, A. M. Echavarren, M. C. Ramírez de Arellano, *Organometallics* **1999**, *18*, 3337 – 3341.

[8] G. M. Kapteijn, D. M. Grove, H. Kooijman, W. J. J. Smeets, A. L. Spek, G. van Koten, *Inorg. Chem.* **1996**, *35*, 526 – 533.

[9] a) T. N. Singh-Rachford, F. N. Castellano, *Coord. Chem. Rev.* **2010**, *254*, 2560 – 2573.

[10] a) T. P. Yoon, M. A. Ischay, J. Du, *Nat. Chem.* **2010**, *2*, 527 – 532; b) J. M. R. Narayanam, C. R. J. Stephenson, *Chem. Soc. Rev.* **2011**, *40*, 102 – 113; c) L. Shi, W. Xia, *Chem. Soc. Rev.* **2012**, *41*, 7687 – 7697.

[11] a) M. C. DeRosa, R. J. Crutchley, *Coord. Chem. Rev.* **2002**, *233*, 351 – 371; b) W.-P. To, Y. Liu, T.-C. Lau, C.-M. Che, *Chem. Eur. J.* **2013**, *19*, 5654 – 5664.

[12] X. Yang, C. Yao, G. Zhou, *Platinum Met. Rev.* **2013**, *57*, 2 – 16.

